Physics of the Earth and Planetary Interiors 208-209 (2012) 11–24

Contents lists available at SciVerse ScienceDirect

Physics of the Earth and Planetary Interiors

journal homepage: www.elsevier.com/locate/pepi

The viscosity structure of the D″ layer of the Earth's mantle inferred from the analysis of Chandler wobble and tidal deformation

Masao Nakada [a,*], Chihiro Iriguchi [b], Shun-ichiro Karato [c]

[a] Department of Earth and Planetary Sciences, Faculty of Science, Kyushu University, Fukuoka 812-8581, Japan
[b] Department of Earth and Planetary Sciences, Graduate School of Sciences, Kyushu University, Fukuoka 812-8581, Japan
[c] Department of Geology and Geophysics, Yale University, New Haven, CT 06520, USA

ARTICLE INFO

Article history:
Received 31 March 2012
Received in revised form 29 June 2012
Accepted 2 July 2012
Available online 14 July 2012
Edited by Kei Hirose

Keywords:
Chandler wobble
Tidal deformation
D″ layer
Core–mantle boundary
Viscosity
Maxwell body

ABSTRACT

The viscosity structure of the D″ layer of the Earth's mantle is inferred from the decay time of the Chandler wobble and semi-diurnal to 18.6 years tidal deformations combined with model viscosity–depth profiles corresponding to a range of temperature–depth models. We use two typical temperature profiles of the D″ layer by considering its dynamic state: (i) bottom thermal boundary layer of the mantle convection (TBL model) and (ii) vigorously small-scale convecting layer (CON model). Three possible models are derived from the comparison between the numerical and observationally inferred decay times of Chandler wobble and tidal deformation. The first and second models are those with a viscosity of $\sim 10^{16}$ Pa s at the core–mantle boundary. The temperature gradient for the first one, TBL model with a thickness of the D″ layer (L) of ~200 km, is nearly constant within the D″ layer. The second one, TBL and CON models with $L \sim 300$ km, requires that the temperature gradient of the lower part (~100 km thickness) is larger than that of the upper part. The temperature increases within the D″ layer for these two models are larger than ~1500 K. The third model has a constant low viscosity layer (~100 km thickness and viscosity smaller than $\sim 10^{17}$ Pa s) at the bottom of the D″ layer in TBL ($L \sim 200$ and 300 km) and CON ($L \sim 300$ km) models. The temperature increases would be 1000–1600 K depending on the viscosity at the top of the D″ layer (10^{21}–10^{22} Pa s). The heat flows from the core to the mantle for these three models are estimated to be larger than ~5 TW. The third model may be preferable after comprehensively taking account of the fitness of the decay time of the Chandler wobble and the tidal deformations for each model.

1. Introduction

D″ layer of the Earth's mantle, the lowermost layer in the Earth's mantle, plays an important role in the dynamics and evolution of the Earth. In particular, its rheological properties are important in discussing a number of geodynamic processes, but it is difficult to estimate its viscosity structure based on commonly used methods, glacial isostatic adjustment (GIA) due to the last deglaciation (Peltier and Andrews, 1976) and flow models inferred from global long geoid anomalies (Hager, 1984). The GIA observations for the relative sea level (RSL) during the postglacial phase have little sensitivity to the viscosity of the mantle deeper than ~1200 km (Mitrovica and Peltier, 1991). In the latter approach, Earth's surface gravity signals are used to estimate the viscous response to the lateral density variations inside the mantle inferred from seismic tomography (Hager, 1984; Hager et al., 1985). The approach is, in principle, effective in estimating the viscosity structure for the whole mantle, but the velocity-to-density conversion factor is uncertain in the deep mantle such as the D″ layer where the temperature sensitivity of seismic wave velocities decreases due to high pressure, and also chemical heterogeneity may cause velocity heterogeneity (Karato and Karki, 2001; Karato, 2008).

More recently, Nakada and Karato (2012) showed that the decay time of the Chandler wobble and tidal deformation with typical periods longer than ~0.1 year, which are related to the deformation in the deep mantle (Smith and Dahlen, 1981), can be interpreted as viscoelastic responses for the Maxwell body (e.g., Peltier, 1974) and also provide new constraints on the rheological properties of the D″ layer. Regarding the excitation of the Chandler wobble, there is growing consensus that the source is a combination of atmospheric, oceanic and hydrologic processes (e.g., Gross, 2007). Once the Chandler wobble is excited, the amplitude of Chandler wobble decays with a decay time of $\tau_{CW} = 2Q_{CW}T_{CW}/2\pi$ in the absence of excitation, in which T_{CW} and Q_{CW} are the period and quality factor of Chandler wobble, respectively (e.g., Munk and Macdonald, 1960; Smith and Dahlen, 1981). The values of

* Corresponding author. Tel.: +81 92 642 2515; fax: +81 92 642 2684.
E-mail addresses: mnakada@geo.kyushu-u.ac.jp (M. Nakada), 2SC11121Y@s.kyushu-u.ac.jp (C. Iriguchi), shun-ichiro.karato@yale.edu (S.-i. Karato).

0031-9201/$ - see front matter © 2012 Elsevier B.V. All rights reserved.
http://dx.doi.org/10.1016/j.pepi.2012.07.002

T_{CW} and Q_{CW}, recently reviewed and recommended by Gross (2007), are: T_{CW} of 433 ± 1.1 (1 σ) sidereal days and Q_{CW} of 179 with a 1σ range of 74–789 estimated by Wilson and Vicente (1990), corresponding to the decay times of 30–300 years.

We briefly summarize the results by Nakada and Karato (2012). The decay time of Chandler wobble provides information on the effective viscosity of the D″ layer with the thickness of ~300 km. Moreover, the viscosity of the bottom part of ~100 km thickness is constrained more tightly by using the tidal deformations across the semi-diurnal to 18.6 years tides as well. These deformations combined with the GIA constraints by relative sea level observations suggest that the effective viscosity of the D″ layer (~300 km thickness) is 10^{19}–10^{20} Pa s, and that for the bottom part of the D″ layer (~100 km thickness) is less than 10^{18} Pa s.

The estimates by Nakada and Karato (2012) are, however, based on simple one- or two-layer viscosity model. If we consider that the temperature gradient is likely high in the D″ layer as inferred from the double-crossing of seismic rays of the phase boundary between perovskite and post-perovskite (Hernlund et al., 2005) and the viscosity is highly sensitive to temperature (e.g., Karato, 2008), then it is important to examine these deformation processes based on the models with temperature (T) dependent viscosity structure. In examining these deformation processes based on a T-dependent viscosity model, we adopt two typical temperature profiles by considering that the D″ layer is a bottom thermal boundary layer of the mantle convection (e.g., Turcotte and Schubert, 1982), or vigorous small-scale convection occurs in the D″ layer (Solomatov and Moresi, 2002). These numerical results are discussed in Sections 3 and 4, respectively. The present results, consequently, provide important constraints on both the depth-dependent viscosity structure of the D″ layer, temperature of the core–mantle boundary (CMB) (Boehler, 2000; Alfè et al., 2002) and heat flow from the core to mantle (e.g., Lay et al., 2008). We discuss these points in Section 5.

2. Numerical method

Here we adopt the Maxwell viscoelastic Earth's model, and briefly explain the method to estimate the decay time of Chandler wobble and the response function to tidal forcing (Nakada and Karato, 2012). The density and elastic constants are based on the PREM (Dziewonski and Anderson, 1981) model. The thickness of elastic lithosphere is 100 km and upper mantle viscosity is 10^{21} Pa s. The lower mantle viscosity above the D″ layer is assumed to be 10^{22} Pa s. This model is similar to a rheological model explaining relative sea level observations for the postglacial rebound around the Australian region (Nakada and Lambeck, 1989). However, the choice of the background model does not affect the conclusions on the viscosity of the lowermost layer of the mantle so much.

The Chandler wobble is simulated by a linearized Liouville equation describing the polar motion $m = m_1 + im_2$ ($|m_i| << 1$) using the Maxwell model, where the quantities m_1 and m_2 describe the displacement of the rotation axis in the directions 0° and 90°E, respectively (e.g., Sabadini and Peltier, 1981; Wu and Peltier, 1984):

$$i\frac{\dot{\mathbf{m}}(t)}{\sigma_r} + \mathbf{m}(t) = \frac{1}{C-A}(\delta(t) + k^{L}(t)) * \left(\Delta \mathrm{I}(t) - i\frac{\Delta \dot{\mathrm{I}}(t)}{\Omega}\right) + \frac{k^{T}(t)}{k_f} * \mathbf{m}(t) \quad (1)$$

where asterisk (∗) denotes convolution, $\delta(t)$ is the delta function, Ω is the mean angular velocity of the Earth, $\sigma_r = (C-A)\Omega/A$, $\Delta\mathbf{I} = \Delta I_{13}(t) + i\Delta I_{23}(t)$, A and C are the equatorial and polar moments of inertia, respectively. $\Delta I_{13}(t)$ and $\Delta I_{23}(t)$ are forcing inertia elements for the polar motion. Love numbers $k^{L}(t)$ and $k^{T}(t)$ in Eq. (1) depend on the density and viscoelastic structure of the Earth, and characterize the time-dependent Earth deformation to surface loading and that to the potential perturbation, respectively (Peltier, 1974). k_f is the fluid Love number characterizing the hydrostatic state of the Earth and is defined by $3G(C-A)/(a^5\Omega^2)$, where G is the gravitational constant (Munk and MacDonald, 1960). We numerically simulate the Chandler wobble excited by the pulse-like forcing function of $\Delta I_{13}(t)$ and $\Delta I_{23}(t)$ and estimate its decay time (Nakada, 2009; Nakada and Karato, 2012).

The deformation by the luni-solar tidal force is sensitive to the anelastic properties of deep mantle (Smith and Dahlen, 1981), and the responses to the forcings with periods longer than ~0.1 year can be examined based on the Maxwell viscoelastic model Nakada and Karato, 2012). Here we do not consider the effects of the core–mantle coupling such as electromagnetic coupling (Buffett et al., 2002). Then, the Earth's response $R(\omega,t)$ to a periodic forcing of $F(\omega,t) \propto e^{i\omega t}$ with frequency ω is given by $R(\omega,t) = k^{T}(t) * F(\omega,t)$ using the tidal Love number $k^{T}(t)$, and $k^{T,P}(\omega)F(\omega,t)$ (Lambeck and Nakiboglu, 1983; Sabadini et al., 1985). The Love number, $k^{T,P}(\omega)$, takes a complex form of $k^{T,P}(\omega) = k_r^{T,P}(\omega) + ik_i^{T,P}(\omega)$, and depends on the viscoelastic structure, particularly on the viscosity structure of the deep mantle. The amplitude of the response is characterized by its modulus, $|k^{T,P}|$, and the phase difference between the response and forcing, $\Delta\phi$, is given by $\Delta\phi = \tan^{-1}(-k_i^{T,P}/k_r^{T,P})$. That is, we can estimate the Love number as a function of frequency by analyzing the time series of geodetic observations, $R(\omega,t)$.

In order to discuss the decay time of the Chandler wobble and tidal deformations, we adopt the T-dependent viscosity structure, $\eta(z)$, for the D″ layer given by:

$$\eta(z) = \eta_0 \exp(H^*/RT) \quad (2)$$

where z is the depth and H^* is the activation enthalpy (e.g., Karato, 2008). The depth of the top of the D″ layer is z_{top} and that for the bottom is given by z_{CMB}, and therefore the thickness of the D″ layer, L, is $L = z_{CMB} - z_{top}$. In the PREM model with $z_{CMB} = 2891$ km, $L = 300$ km for $z_{top} = 2591$ km. Here we put $\eta(z_{top}) = \eta_{top}$ and $T(z_{top}) = T_{top}$. Then we get $\eta_0 = \eta_{top}\exp(-H^*/RT_{top})$, and Eq. (2) is consequently expressed as:

$$\eta(z) = \eta_{top} \exp\left[-\frac{H^*}{R}\left(\frac{1}{T_{top}} - \frac{1}{T(z)}\right)\right] \quad (3)$$

Here we put $T(z) = T_{top} + \Delta T(z)$, then Eq. (3) takes a form of:

$$\eta(z) = \eta_{top} \exp\left(-\frac{H^*}{RT_{top}} \frac{\Delta T(z)/T_{top}}{1 + \Delta T(z)/T_{top}}\right) \quad (4)$$

Eq. (4) is used to estimate the depth-dependent viscosity structure, which is a function of η_{top}, H^*/RT_{top} and $\Delta T/T_{top}$. Also we denote the viscosity and temperature increase at the base of the D″ layer as $\eta(z_{CMB}) = \eta_{CMB}$ and $\Delta T(z_{CMB}) = \Delta T_{CMB}$, then we get:

$$\eta_{CMB} = \eta_{top} \exp\left(-\frac{H^*}{RT_{top}} \frac{\Delta T_{CMB}/T_{top}}{1 + \Delta T_{CMB}/T_{top}}\right) \quad (5)$$

Eq.(5) is also written as:

$$In\frac{\eta_{top}}{\eta_{CMB}} = \frac{H^*}{RT_{top}} \frac{\Delta T_{CMB}/T_{top}}{1 + \Delta T_{CMB}/T_{top}} \quad (6)$$

The relationship between H^*/RT_{top} and $\Delta T_{CMB}/T_{top}$ given by Eq. (6) is used to discuss the temperature at the CMB in Section 5.

3. Results for a bottom thermal boundary layer model

3.1. Setting of parameter values

The viscosity structure of the D″ layer is derived from Eq. (4) by giving values of η_{top}, T_{top}, H^* and depth-dependent $\Delta T(z)$. Firstly, the temperature gradient, dT/dz, is assumed to be constant for the whole D″ layer, i.e., $dT/dz = a$ (constant). Then we get the viscosity structure for $\Delta T(z) = a(z - z_{top})$ at an arbitrary depth. In this study, however, we examine the decay time of the Chandler wobble and tidal deformations (two data sets) as a function of viscosity at the base of D″ layer η_{CMB}, using a relationship of Eq. (6) that the temperature gradient is determined for given values of η_{top}, T_{top}, H^* and η_{CMB}. For numerical calculations, we divide the D″ layer into a number of sub-layers with constant thickness and viscosity, and the viscosity of each sub-layer is fixed to the value at the mid-depth. According to numerical experiments with the thickness of 25 and 50 km, differences of the predictions for two data sets are less 1% for a model with 300 km thickness of D″ layer (L) regardless of the values of η_{CMB}. In cases of L = 200 and 250 km, we also get sufficiently accurate predictions for a model with 25 km thickness, and therefore the sub-layer thickness is fixed to 25 km.

The viscosity profiles for TBL1 model (see Table 1) are shown in Fig. 1 as a function of viscosity at the base of the D″ layer η_{CMB} for a model with H^* = 500 kJ mol^{-1}, T_{top} = 2600 K, $\eta_{top} = 10^{22}$ Pa s and L = 300 km, and Fig. 2 shows the predicted decay times of the Chandler wobble for each model. The temperature above the D″ layer is assumed to be adiabatic. The value of H^* corresponds to that by Yamazaki and Karato (2001) and the uncertainty is ~100 kJ mol^{-1}. The depth-dependent temperature distribution for a specific valueη_{CMB}, for example, $\eta_{CMB} = 2 \times 10^{18}$ Pa s, is affected by the uncertainties of H^* and T_{top}, which may significantly affect the predictions for two data sets. Here we have examined two data sets based on the viscosity models with H^* = 400, 500 and 600 kJ mol^{-1} and T_{top} = 2600, 2900 and 3200 K, in which η_{CMB} is fixed to a specific value. Although we do not show the results here, the differences are negligibly small and those for the decay time of Chandler wobble are several years at most. We therefore show the predictions for H^* = 500 kJ mol^{-1} and T_{top} = 2600 K.

In this study, we adopt $\eta_{top} = 10^{21}$ and 10^{22} Pa s. The results for $\eta_{top} > 10^{22}$ Pa s are inferred from those for $\eta_{top} = 10^{22}$ Pa s. On the other hand, the conclusions for the viscosity structure of the D″ layer with $\eta_{top} \sim 10^{20}$ Pa s are essentially the same as those for a uniform one-layer model adopted by Nakada and Karato (2012),

Table 1
Temperature and viscosity structures of the D″ layer for a bottom thermal boundary layer model (TBL model). The bottom of the D″ layer is 2891 km depth and the thickness of the lower layer is 100 km. The temperature gradients for the upper and lower layers are denoted by $(dT/dz)_u$ (constant) and $(dT/dz)_l$ (constant), respectively. In these models, the lithospheric (elastic) thickness is 100 km, and the upper and lower mantle viscosities except for the D″ layer are 10^{21} and 10^{22} Pa s, respectively. The viscosity of 2291–2591 km depth is 10^{21} Pa s for TBL3 model.

Model name	Thickness of the D″ layer (km)	Viscosity at the top of the D″ layer (η_{top}) (Pa s)	Viscosity of the lower layer (100 km thickness) of the D″ layer	Temperature gradient structure
TBL1	300	10^{22}	variables	$(dT/dz)_u = (dT/dz)_l$
TBL2	300	10^{21}	variables	$(dT/dz)_u = (dT/dz)_l$
TBL3	300	10^{21}	variables	$(dT/dz)_u = (dT/dz)_l$
TBL4	200	10^{22}	variables	$(dT/dz)_u = (dT/dz)_l$
TBL5	200	10^{21}	variables	$(dT/dz)_u = (dT/dz)_l$
TBL1a	300	10^{22}	10^{16} Pa s at the bottom	$(dT/dz)_u < (dT/dz)_l$
TBL1b	300	10^{22}	10^{17} Pa s at the bottom	$(dT/dz)_u < (dT/dz)_l$
TBL2a	300	10^{21}	10^{16} Pa s at the bottom	$(dT/dz)_u < (dT/dz)_l$
TBL2b	300	10^{21}	10^{17} Pa s at the bottom	$(dT/dz)_u < (dT/dz)_l$
TBL1c	300	10^{22}	5×10^{16} Pa s for 2791–2891 km depth	$(dT/dz)_u$, $(dT/dz)_l = 0$
TBL1d	300	10^{22}	10^{17} Pa s for 2791–2891 km depth	$(dT/dz)_u$, $(dT/dz)_l = 0$
TBL1e	300	10^{22}	2×10^{17} Pa s for 2791–2891 km depth	$(dT/dz)_u$, $(dT/dz)_l = 0$
TBL1f	300	10^{22}	5×10^{17} Pa s for 2791–2891 km depth	$(dT/dz)_u$, $(dT/dz)_l = 0$
TBL2c	300	10^{21}	5×10^{16} Pa s for 2791–2891 km depth	$(dT/dz)_u$, $(dT/dz)_l = 0$
TBL2d	300	10^{21}	10^{17} Pa s for 2791–2891 km depth	$(dT/dz)_u$, $(dT/dz)_l = 0$
TBL4c	200	10^{22}	5×10^{16} Pa s for 2791–2891 km depth	$(dT/dz)_u$, $(dT/dz)_l = 0$
TBL4d	200	10^{22}	10^{17} Pa s for 2791–2891 km depth	$(dT/dz)_u$, $(dT/dz)_l = 0$
TBL4f	200	10^{22}	5×10^{17} Pa s for 2791–2891 km depth	$(dT/dz)_u$, $(dT/dz)_l = 0$
TBL5c	200	10^{21}	5×10^{16} Pa s for 2791–2891 km depth	$(dT/dz)_u$, $(dT/dz)_l = 0$
TBL5d	200	10^{21}	10^{17} Pa s for 2791–2891 km depth	$(dT/dz)_u$, $(dT/dz)_l = 0$

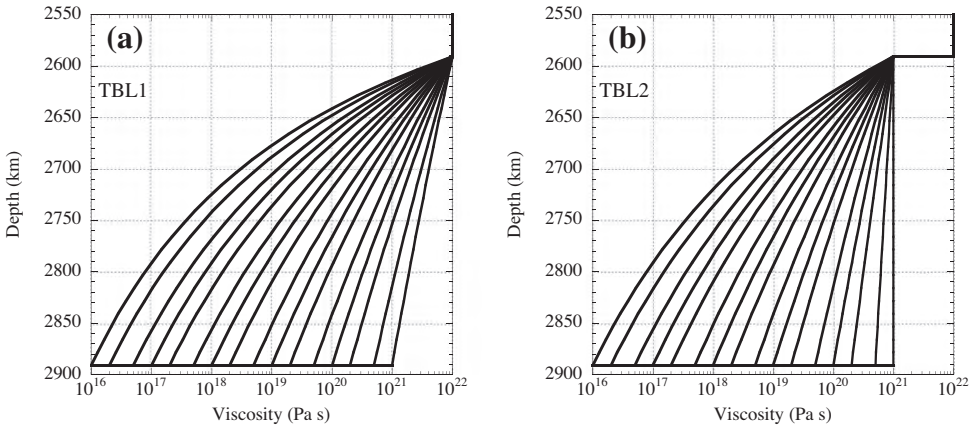

Fig. 1. Viscosity profiles for the D″ layer of TBL1 and TBL2 models with H^* = 500 kJ mol^{-1} and T_{top} = 2600 K.

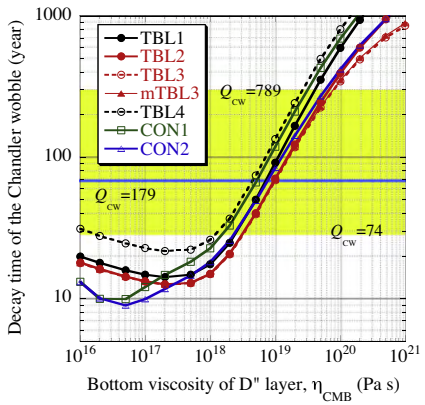

Fig. 2. Decay times of the Chandler wobble for several viscosity models as a function of the bottom viscosity of the D″ layer η_{CMB} and the estimates for $74 \leqslant Q_{CW} \leqslant 789$ by Wilson and Vicente (1990). The parameter values for each model are shown in Tables 1 and 2. In mTBL3 model, the viscosity for 1491–2091 km depth range is 10^{23} Pa s and the viscosity structure except for this depth range is the same as that for TBL3.

which approximately corresponds to a convecting D″ layer model (see Section 4) with very thin upper and lower thermal boundary layers. In a model of TBL2 with $\eta_{top} = 10^{21}$ Pa s (Table 1 and Fig. 1a for the viscosity structure of the D″ layer), the viscosity at $z = z_{top}$ is discontinuous. To examine the effect of this jump on the decay time, we compute the decay times of the Chandler wobble for a model with the lower mantle viscosity of 10^{22} Pa s for $670 \leqslant z < 2291$ km depth and 10^{21} Pa s for $2291 \leqslant z < 2591$ km depth (TBL3 in Table 1). The difference in the decay times between models TBL2 and TBL3 is detected for $\eta_{CMB} > 5 \times 10^{19}$ Pa s (Fig. 2). However, the permissible viscosity range for observationally inferred decay times of 30–300 years (Wilson and Vicente, 1990) is similar for the viscosity structures TBL2 and TBL3. We therefore adopt TBL2 in the case of $\eta_{top} = 10^{21}$ Pa s.

Here we shortly comment about the effect of a non-uniform lower mantle viscosity profile with viscosity $\sim 10^{23}$ Pa s around 1800 km depth (e.g., Mitrovica and Forte, 2004) on the decay time of the Chandler wobble. We adopt a viscosity model of mTBL3, in which the viscosity for $1491 \leqslant z < 2091$ km depth is 10^{23} Pa s and the viscosity structure except for this depth range is the same as that for TBL3. The difference in the decay times between mTBL3 and TBL3 models shown in Fig. 2 is negligibly small, suggesting that such viscosity stratification of the lower mantle does not alter the results presented here (see also Nakada and Karato (2012)).

3.2. Inference of the D″ viscosity structure based on a constant temperature gradient

Fig. 2 shows the decay times of the Chandler wobble (τ_{CW}) for models TBL1 ($\eta_{top} = 10^{22}$ Pa s) and TBL2 ($\eta_{top} = 10^{21}$ Pa s) with the D″ layer of 300 km thickness, in which the region with viscosity larger than $\sim 5 \times 10^{20}$ Pa s insignificantly affects the decay of the Chandler wobble (Nakada and Karato, 2012). Although we do not show here, the decay times for $\eta_{CMB} < 10^{16}$ Pa s are shorter than 30 years. The decay times for observationally inferred Q_{CW}-value by Wilson and Vicente (1990) are 30–300 years with the optimum values of $Q_{CW} = 179$ and 68 years. For models TBL1 and TBL2, permissible values of η_{CMB} satisfying the decay times of 30–300 yeas are $3 \times 10^{18} \leqslant \eta_{CMB} \leqslant 4 \times 10^{19}$ Pa s and $4 \times 10^{18} \leqslant \eta_{CMB} < 7 \times 10^{19}$ Pa s, and η_{CMB}-values for $\tau_{CW} = 68$ years are $\sim 8 \times 10^{18}$ and $\sim 10^{19}$ Pa s, respectively. These results indicate that the decay times are less sensitive to the η_{top}-value adopted here.

To examine the effect of thickness of the D″ layer (L) on the decay time, we have evaluated the decay times for $L = 300$, 250 and 200 km. The thicknesses of 300 km and 200 km may correspond to 'cold' and 'hot' mantle by Hernlund et al. (2005), respectively. The decay times for models TBL4 with $L = 200$ km are shown in Fig. 2, and permissible values of η_{CMB} satisfying τ_{CW} of 30–300 years naturally decrease with decreasing the thickness (Nakada and Karato, 2012). Consequently, TBL4 model with $\eta_{CMB} \sim 10^{16}$ Pa s predicts the decay time of ~ 30 years (also TBL5 model shown in Fig. 6b), corresponding to the observationally inferred minimum estimate. For these predictions, we should note that the functional type of decay time as a function of η_{CMB} takes a similar form of parabola as indicated by Nakada and Karato (2012). This reflects that the decay of the Chandler wobble is mainly determined by the upper part: when the lower part with a viscosity smaller than $\sim 10^{17}$ Pa s behaves as an inviscid layer to the deformation for the Chandler wobble (see also Fig. 8 for a simple two-layer viscosity model by Nakada and Karato (2012)).

We next discuss the tidal responses described by the real part, $k_r^{T,P}$, and the imaginary part, $k_i^{T,P}$, of the Love numbers. The Love numbers examined here are geodetically inferred Love numbers for semi-diurnal (M_2) (Ray et al., 2001), nine-day (M_9) (Dickman and Nam, 1998), fortnightly (M_f) (Dickman and Nam, 1998; Benjamin et al., 2006), monthly (M_m) (Dickman and Nam, 1998; Benjamin et al., 2006), 18.6 years tide (Benjamin et al., 2006) and Chandler wobble corrected for the ocean effects (Dickman and Nam, 1998; Benjamin et al., 2006) (Fig. 3). The estimates for Chandler wobble correspond to the response to the accompanying variations in centrifugal force (e.g., Benjamin et al., 2006). The estimates for 18.6 years tide (Benjamin et al., 2006) are derived from the degree-two and order-zero gravity component for satellite laser ranging from 1979 to 2004.

In these figures, geodetically inferred Love numbers for 18.6 years tide are shown after the correction for several factors (left: after atmospheric effect correction, middle: after atmospheric and oceanic circulation effect correction, right: after the correction used for the middle estimate and continental water + snow + ice effect correction) (Benjamin et al., 2006). These estimates for 18.6 years tide may indicate that the imaginary part is highly sensitive to the correction factors, but not for the real. The left estimate in $k_r^{T,P}$ for the Chandler wobble is for Dickman and Nam (1998). The middle and right estimates in $k_r^{T,P}$ (left and right ones in $k_i^{T,P}$) are based on the original data for Vicente and Wilson (1997) and Furuya and Chao (1996), and the Q_{CW}-values used for the estimates of $k_i^{T,P}$ are 179 and 49, respectively.

The Earth's responses shown in Fig. 3 indicate $|k_i^{T,P}| \ll k_r^{T,P}$ and the real part is dominated by the elastic response, implying that the real part, $k_r^{T,P}$, describes the amplitude response and the phase lag, $\Delta\phi$, is mostly determined by the imaginary part, $k_i^{T,P}$. Although we plot geodetically inferred imaginary parts for the decay times by Vicente and Wilson (1997) (left estimate in Fig. 3) and Furuya and Chao (1996) (right estimate in Fig. 3), we use the decay time by Wilson and Vicente (1990) (Fig. 2) and $k_r^{T,P}$ for the amplitude responses (Fig. 3a and c) in discussing the viscosity structure from the Chandler wobble.

The Love numbers for TBL1 and TBL2 are shown in Fig. 3. The predictions of $k_r^{T,P}$ and $k_i^{T,P}$ for both models (Fig. 3a and b) are nearly identical for periods less than ~ 1 year, and their magnitude of 18.6 years tide for TBL2 ($\eta_{top} = 10^{21}$ Pa s) is only slightly larger than those for TBL1, i.e., at most 0.004 for $k_r^{T,P}$ and $k_i^{T,P}$. However, the numerical experiments indicate that the response amplitude at periods of 18.6 years for TBL2 with a certain value of η_{CMB} is nearly the same as that for TBL1 model with $\sim \eta_{CMB}/2$. For example, we get $k_r^{T,P}$ ($\eta_{CMB} = 10^{18}$ Pa s for TBL2) $\sim k_r^{T,P}$ ($\eta_{CMB} = 5 \times 10^{17}$ Pa s for TBL1) and $k_i^{T,P}$ ($\eta_{CMB} = 10^{18}$ Pa s for TBL2) $\sim k_i^{T,P}$ ($\eta_{CMB} = 5 \times 10^{17}$ Pa s for TBL1). We therefore discuss the viscosity structure of the D″ layer based on the Love numbers for viscosity models with $\eta_{top} = 10^{22}$ Pa s.

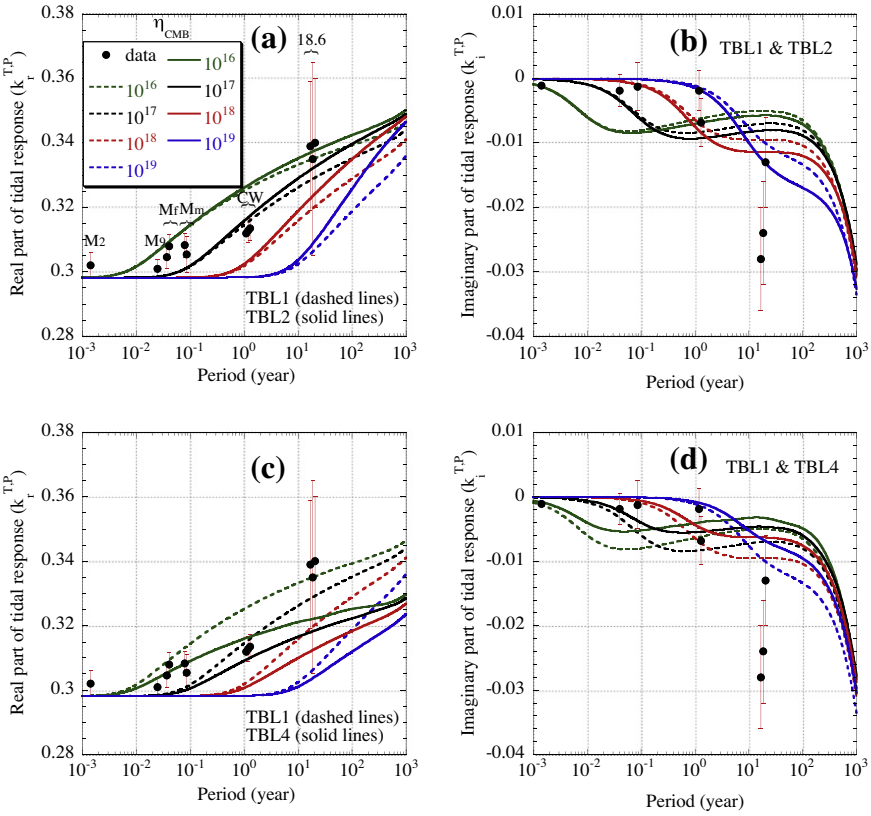

Fig. 3. Real (a, c) and imaginary (b, d) parts of tidal responses for TBL1, TBL2 and TBL4 models and geodetically inferred estimates for semi-diurnal tide (M_2) (Ray et al., 2001), nine-day tide (M_9) (Dickman and Nam, 1998), fortnightly tide (M_f) (Dickman and Nam, 1998; Benjamin et al., 2006), monthly tide (M_m) (Dickman and Nam, 1998; Benjamin et al., 2006), Chandler wobble (Dickman and Nam, 1998; Benjamin et al., 2006) and 18.6 years tide (Benjamin et al., 2006) as a function of the period. To clearly show each estimate, we plot the data with appropriate shift of position of the period. The estimates for 18.6 years tide were derived from the degree two ($n = 2$) and order zero ($m = 0$) gravity component for satellite laser ranging (SLR) from 1979 to 2004 (26 years). These data include the effects associated with atmospheric, oceanic and hydrologic processes. The left, middle and right estimates are corrected for atmospheric effects, atmospheric and ocean circulation effects, and atmospheric, ocean circulation and continental water + snow + ice effects, respectively (Benjamin et al., 2006). In the estimates for the Chandler wobble, the left estimate in $k_r^{T,P}$ is for Dickman and Nam (1998). The middle and right estimates in $k_r^{T,P}$ (left and right ones in $k_i^{T,P}$) are based on the original data for Vicente and Wilson (1997) and Furuya and Chao (1996), and the Q_{CW}-values used for the estimates of $k_i^{T,P}$ are 179 and 49, respectively.

Fig. 3c and d show the responses for TBL1 and TBL4, in which the thicknesses of the D″ layer (L) are 300 and 200 km, respectively. We do not show the results for 250 km thickness because the results are intermediate between these predictions. The results for $k_r^{T,P}$ are significantly sensitive to its thickness, and the magnitude at periods ∼1.2 and 18.6 years for TBL4 is ∼0.01 and ∼0.015 smaller than that for TBL1, respectively. The magnitude of $k_i^{T,P}$ for TBL4 is also smaller than that for TBL1. That is, the viscoelastic Earth's responses for periods examined here are approximately proportional to the thickness of viscoelastic D″ layer for viscosity models with an identical CMB viscosity (η_{CMB}), and the magnitude for TBL4 is ∼2/3 for that of TBL1. This relationship is also true for the predictions of $k_r^{T,P}$ and $k_i^{T,P}$ between TBL2 and TBL5 with $\eta_{top} = 10^{21}$ Pa s (see Table 1).

As discussed by Nakada and Karato (2012), the deformations for periods longer than ∼0.1 year are interpreted as the viscoelastic responses for the Maxwell model. That is, the responses for the Chandler wobble and 18.6 years tide would be explained by the responses examined here. In the real part of Love number, $k_r^{T,P}$, for TBL1 and TBL2 models, the permissible range of η_{CMB} for 18.6 years tide is $\eta_{CMB} \leqslant 10^{18}$ Pa s, and that for the Chandler wobble is $\eta_{CMB} \sim 10^{17}$ Pa s (Fig. 3a). The η_{CMB}-value of $\sim 10^{17}$ Pa s satisfying these deformations is, however, significantly smaller than the viscosity inferred from the decay times as shown in Fig. 2. Consequently, Nakada and Karato (2012) has proposed a low viscosity zone with $\sim 10^{17}$ Pa s and ∼100 km thickness at the base of the D″ layer to resolve the discrepancy for two data sets.

On the other hand, the responses for $k_r^{T,P}$ at periods longer than ∼0.1 year can be explained by TBL4 model with $\eta_{CMB} \sim 10^{16}$ Pa s, which also predicts the decay time of ∼30 years for the minimum estimate by Wilson and Vicente (1990). However, this model cannot explain the imaginary part. This is true for a viscosity model of TBL5 with $\eta_{top} = 10^{21}$ Pa s. We will discuss geophysical implications for these models in Section 5.

In the next section, we examine two data sets based on the viscosity models with depth-dependent temperature gradients for the D″ layer, and also examine whether a low viscosity zone at the very bottom of the D″ layer proposed by Nakada and Karato (2012) is required in explaining both data sets simultaneously.

3.3. Inference of the D″ viscosity for models with depth-dependent temperature gradients and constant low viscosity in the lower part of the D″ layer

In this section, we examine two cases, (i) different temperature gradients for the upper and lower parts in the D″ layer, and (ii) inclusion of a constant low viscosity layer at the bottom of the D″ layer. We first examine case (i) for the D″ layer with 300 km thickness only because the depth-dependent temperature gradient is not required for models with 200 km thickness as inferred from

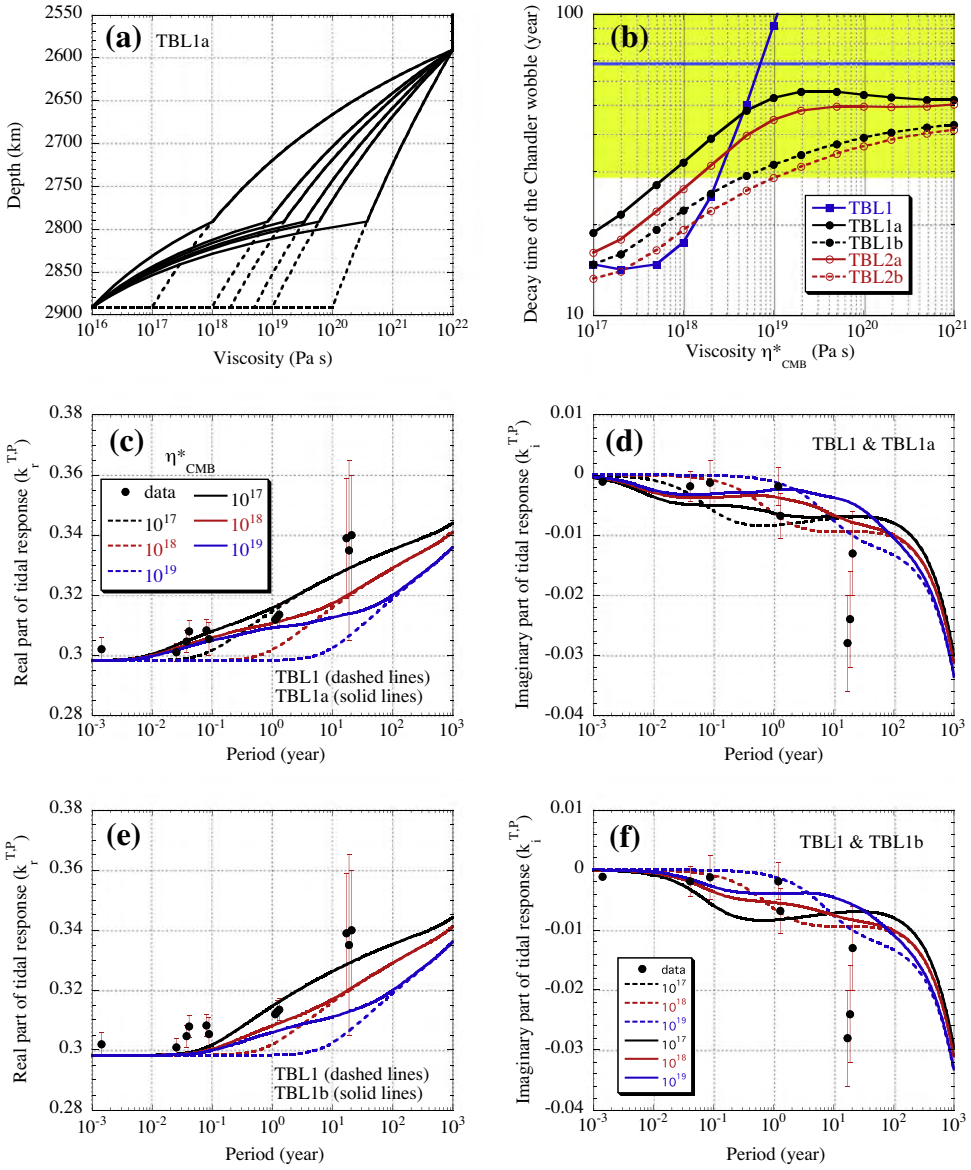

Fig. 4. Results for viscosity models with depth-dependent temperature gradient within the D″ layer. The thickness of the D″ layer is 300 km. (a) Viscosity profiles for TBL1a model, (b) decay times of the Chandler wobble as a function of η^*_{CMB} (see text), and real (c), (e) and imaginary (d), (f) parts of tidal responses as a function of period. The parameter values for each model are shown in Table 1.

the results for TBL4 model. The boundary depths (z_b) of a change in temperature gradient (dT/dz) are assumed to be 2791 and 2691 km, and we have examined two cases of these models. The viscosity distribution for the upper layer ($z \leqslant z_b$) is determined by giving the CMB viscosity as for models of TBL1 and TBL2, and that for the lower layer ($z > z_b$) is derived from the viscosity at $z = z_b$, $\eta(z_b)$, and a specific viscosity of the CMB (η_{CMB}), 10^{16} or 10^{17} Pa s. The temperature gradients are assumed to be constant in each layer. The temperature profile for this model is similar to a model by Hernlund et al. (2005) studying a doubling of the post-perovskite phase boundary in the D″ layer for the 'cold' mantle.

Fig. 4a shows the viscosity profiles of TBL1 (dashed lines) and TBL1a (solid lines) with $\eta_{top} = 10^{22}$ Pa s and $\eta_{CMB} = 10^{16}$ Pa s. The TBL1a model has a more distinct low viscosity zone relative to that for TBL1. The viscosity profile of TBL1a is characterized by the values of η_{top} and η_{CMB}, and also an extrapolated CMB viscosity, η^*_{CMB}, corresponding to the CMB viscosity for the TBL1 with a constant dT/dz value for the whole layer. Fig. 4b shows the decay times of the Chandler wobble for models TBL1a, TBL1b ($\eta_{CMB} = 10^{17}$ Pa s), TBL2a and TBL2b (Table 1). The decay time becomes longer with decreasing η_{CMB}-value, implying that the decay is predominantly controlled by the viscous response for the upper layer as the lower layer becomes inviscid in terms of the decay of the Chandler wobble (Nakada and Karato, 2012). The η^*_{CMB}-values for models satisfying observationally inferred decay times are $\eta^*_{CMB} \geqslant 8 \times 10^{17}$ Pa s for TBL1a and $\eta^*_{CMB} \geqslant 6 \times 10^{18}$ Pa s for TBL1b. Although we do not show the results for models with a boundary depth of 2691 km, the decay times for those models are shorter than 30 years and cannot explain the observationally inferred decay times.

Fig. 4c–f show the predictions for $k_r^{T,P}$ and $k_i^{T,P}$ for TBL1, TBL1a and TBL1b. Differences of the predictions between TBL1, TBL1a and TBL1b are clearly seen in the predicted $k_r^{T,P}$. The magnitude of $k_r^{T,P}$ at periods less than 10–100 years for TBL1a and TBL1b is larger than that for TBL1 and its effect reaches to much shorter period range decreasing η_{CMB}-value. Consequently, the geodetically inferred tidal deformations of $k_r^{T,P}$ for 0.01∼0.1 year can be explained by the predictions for TBL1a with $\eta_{CMB} = 10^{16}$ Pa s. Although it may be difficult to clearly describe the differences for predicted $k_i^{T,P}$, the

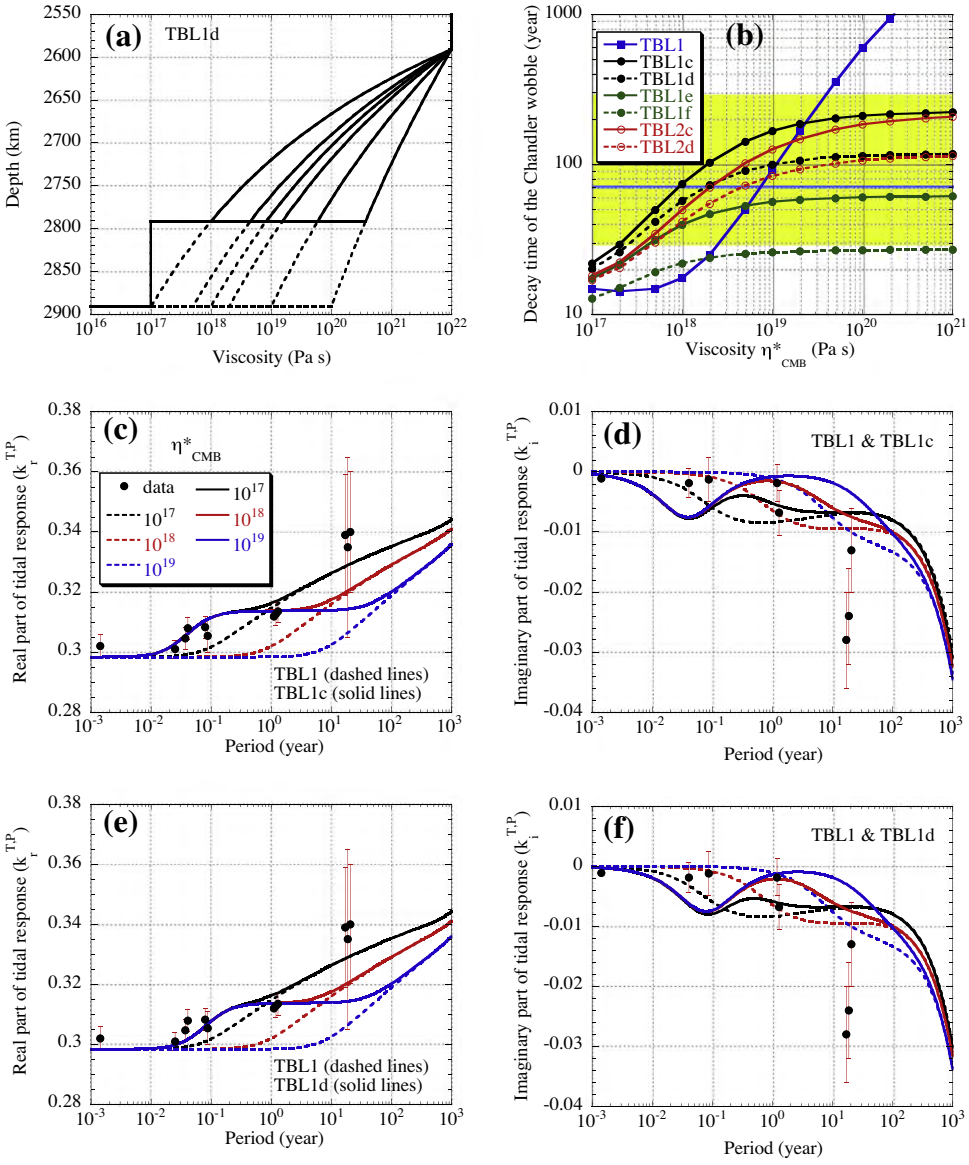

Fig. 5. Results for viscosity models with a constant low viscosity layer at the bottom of the D″ layer. The thicknesses of the D″ layer and the constant viscosity layer are 300 and 100 km, respectively. (a) Viscosity profiles for TBL1d model, (b) decay times of the Chandler wobble as a function of η^*_{CMB} (see text), and real (c), (e) and imaginary (d), (f) parts of tidal responses as a function of period. The parameter values for each model are shown in Table 1.

magnitude of $k_i^{T,P}$ at a period of 18.6 years becomes smaller than that for TBL1. These characteristics for $k_r^{T,P}$ and $k_i^{T,P}$ are caused by a more distinct low viscosity zone relative to that for TBL1. Consequently, the predictions for TBL1a model ($\eta_{CMB} = 10^{16}$ Pa s) with $\eta^*_{CMB} \sim 10^{18}$ Pa s can explain the geodetically inferred deformations for periods longer than ~0.1 year and also the decay time of the Chandler wobble. The predicted decay time for such a model is, however, ~30 years, corresponding to the minimum estimate by Wilson and Vicente (1990).

Next we discuss two models with a constant viscosity layer at the bottom of the D″ layer (see TBL1d model in Fig. 5a). This model corresponds to a case where the rheological properties are more sensitive to factors other than temperature. We first discuss the results for D″ layer model with 300 km thickness. Fig. 5b depicts the decay times of the Chandler wobble for several models with a constant viscosity layer of 100 km thickness (see Table 1 for the parameter values). Although we have examined based on viscosity models with its thickness of 50 and 100 km, the models with ~100 km thickness are required to explain the tidal deformations as stated below. The η^*_{CMB}-values for models satisfying observationally inferred decay times are $\eta_{CMB} \geqslant 2 \times 10^{17}$ Pa s for TBL1c, $\eta^*_{CMB} \geqslant 3 \times 10^{17}$ Pa s for TBL1d and $\eta^*_{CMB} \geqslant 5 \times 10^{17}$ Pa s for TBL1e, and the predicted decay times for model TBL1f with a constant viscosity (η_{CMB}) of 5×10^{17} Pa s are shorter than the observed estimates. It is noted that TBL1c and TBL1d models, with a developed channel-like low viscosity layer at the bottom of the D″ layer, can predict the decay times of ~70 years corresponding to the optimum value by Wilson and Vicente (1990).

Fig. 5c–f show the $k_r^{T,P}$ and $k_i^{T,P}$ for TBL1, TBL1c and TBL1d, in which the thickness of a constant viscosity layer is 100 km. The value of $k_r^{T,P}$ for such viscosity models is constant for a specific period range and its period range increases with decreasing η_{CMB}-value, which clearly differs from the tendency detected for TBL1a and TBL1b. For example, the $k_r^{T,P}$-value for TBL1c model with $\eta^*_{CMB} = 10^{19}$ Pa s is ~0.315 for 0.1–30 years. For models with 50 km thickness, however, the change of $k_r^{T,P}$ between the elastic one for periods smaller than ~0.01 year and $k_r^{T,P}$ for ~1 year, $\Delta k_r^{T,P}$, is about half for that of 100 km thickness as indicated by

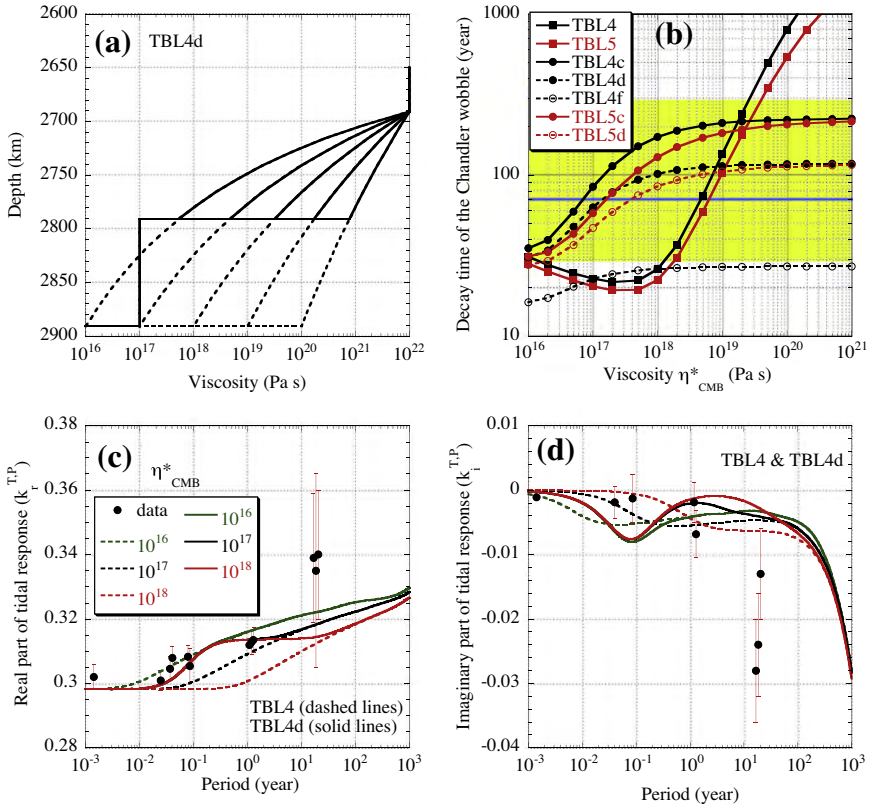

Fig. 6. Results for viscosity models with a constant low viscosity layer at the bottom of the D″ layer. The thicknesses of the D″ layer and the constant viscosity layer are 200 and 100 km, respectively. (a) Viscosity profiles for TBL4d model, (b) decay times of the Chandler wobble as a function of η^*_{CMB} (see text), and real (c) and imaginary (d) parts of tidal responses as a function of period. The parameter values for each model are shown in Table 1.

Nakada and Karato (2012). In the predictions for $k_i^{T,P}$, its magnitude at a period of 18.6 years becomes smaller than that for TBL1. The predicted $k_r^{T,P}$ and $k_i^{T,P}$ for models with $\eta^*_{CMB} \leqslant 10^{18}$ Pa s satisfying observationally inferred decay times are consistent with the geodetically inferred deformations for periods longer than ~0.1 year. Moreover, the decay time for models with $\eta^*_{CMB} \sim 10^{18}$ Pa s is nearly identical to the optimum value by Wilson and Vicente (1990).

We briefly discuss the results for D″ layer model with 200 km thickness. In the models with a constant low viscosity layer of 50 km thickness and viscosityη_{CMB}, the permissible viscosity structure is similar to that for TBL4 model as inferred from the viscosity structure of TBL4d shown in Fig. 6a, i.e., $\eta^*_{CMB} \sim 10^{16}$ Pa s and $\eta_{CMB} \leqslant 10^{17}$ Pa s, and the predicted decay time are also ~30 years. Fig. 6 depicts the results for models with 100 km thickness (see Table 1 for model parameters). Predictions for TBL4c and TBL4d ($\eta_{top} = 10^{22}$ Pa s) with $10^{16} \leqslant \eta^*_{CMB} \leqslant 5 \times 10^{16}$ Pa s can explain observationally inferred decay time of the Chandler wobble and $k_r^{T,P}$, but not $k_i^{T,P}$. The decay times for $\eta^*_{CMB} \sim 5 \times 10^{16}$ Pa s are 40–50 years. For models with $\eta_{top} = 10^{21}$ Pa s (TBL5c and TBL5d), the permissible range is $10^{16} \leqslant \eta^*_{CMB} \leqslant 10^{17}$ Pa s and the decay times for $\eta^*_{CMB} \sim 10^{17}$ Pa s are 60–70 years.

4. Results for a convecting layer model

In case of convecting D″ layer, temperature gradients of the upper and lower thermal boundary layers are significantly higher than that for the interlayer. Here we show the results for models with 100 km thickness for three layers, i.e., upper thermal boundary layer, isothermal layer and bottom thermal boundary layer. Although we have examined several viscosity models with different thickness for each layer, those results are essentially the same as the results shown here. To obtain the temperature distribution for such a convecting D″ layer, we first determine ΔT_{CMB} for a specific value of η_{CMB} using Eq. (6) as for TBL1 and TBL2 models. Then we determine the temperature distributions for both thermal boundary layers by assuming that the gradients for both layers are constant and identical, in which the temperature for the interlayer is fixed to that for the bottom of the upper layer. Fig. 7 shows the viscosity profiles for CON1 model with $\eta_{top} = 10^{22}$ Pa s and CON2 with $\eta_{top} = 10^{21}$ Pa s, and Fig. 2 shows the predicted decay times (τ_{CW}) as a function of η_{CMB} (see Table 2 for convecting D″ layer models). The permissible η_{CMB} values for CON1 and CON2 satisfying τ_{CW}~(30–300) years are $2 \times 10^{18} \leqslant \eta_{CMB} \leqslant 3 \times 10^{19}$ Pa s and $2 \times 10^{18} < \eta_{CMB} \leqslant 6 \times 10^{19}$ Pa s, and η_{CMB}-values for $\tau_{CW} \sim 70$ years are $\sim 5 \times 10^{18}$ Pa s and $\sim 8 \times 10^{18}$ Pa s, respectively. These values are slightly smaller than those for the TBL models.

Fig. 8a and b show the results for $k_r^{T,P}$ and $k_i^{T,P}$ based on TBL1 and CON1 models with several η_{CMB} values. As easily seen, for example, from the differences of $k_r^{T,P}$ for both models with $\eta_{CMB} = 10^{17}$ Pa s, the response for CON1 is more efficient for periods longer than ~3 years and less for smaller than ~3 years. This tendency may be effective to solve the discrepancies for TBL models. However, the predictions for CON1 model satisfying observationally inferred decay times cannot explain the observations with periods longer than ~1 year, which is also true for CON2 model as shown in Fig. 8c and d.

We discuss two data sets based on viscosity models with temperature gradient of the lower layer determined by specific CMB viscosities of 10^{16} and 10^{17} Pa s (η_{CMB}). That is, the temperature gradient of the lower layer is larger than that for the upper layer.

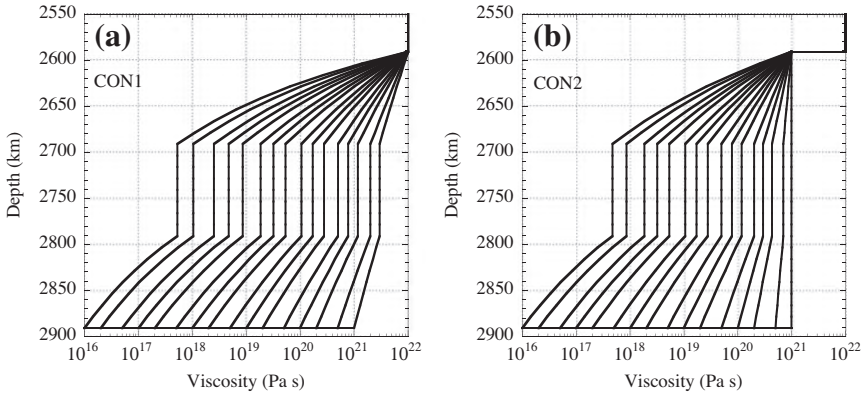

Fig. 7. Viscosity profiles for the D″ layer of CON1 and CON2 models with H^* = 500 kJ mol^{-1} and T_{top} = 2600 K.

Table 2
Temperature and viscosity structures of the D″ layer for a convecting layer model (CON model). The thickness of the D″ layer is 300 km and the bottom of the D″ layer is 2891 km depth. The thickness of the upper and lower thermal boundary layers and the isothermal interlayer is 100 km. The temperature gradients for the upper and lower boundary layers are denoted by $(dT/dz)_u$ (constant) and $(dT/dz)_l$ (constant), respectively. In these models, the lithospheric (elastic) thickness is 100 km, and the upper and lower mantle viscosities except for the D″ layer are 10^{21} and 10^{22} Pa s, respectively.

Model name	Viscosity at the top of the D″ layer (η_{top}) (Pa s)	Viscosity of the lower layer of the D″ layer	Temperature gradient structure
CON1	10^{22}	variables	$(dT/dz)_u = (dT/dz)_l$
CON2	10^{21}	variables	$(dT/dz)_u = (dT/dz)_l$
CON1a	10^{22}	10^{16} Pa s at the bottom	$(dT/dz)_u < (dT/dz)_l$
CON1b	10^{22}	10^{17} Pa s at the bottom	$(dT/dz)_u < (dT/dz)_l$
CON2a	10^{21}	10^{16} Pa s at the bottom	$(dT/dz)_u<(dT/dz)_l$
CON2b	10^{21}	10^{17} Pa s at the bottom	$(dT/dz)_u < (dT/dz)_l$
CON1c	10^{22}	5×10^{16} Pa s for 2791–2891 km depth	$(dT/dz)_u$, $(dT/dz)_l = 0$
CON1d	10^{22}	10^{17} Pa s for 2791–2891 km depth	$(dT/dz)_u$, $(dT/dz)_l = 0$
CON1e	10^{22}	2×10^{17} Pa s for 2791–2891 km depth	$(dT/dz)_u$, $(dT/dz)_l = 0$
CON1f	10^{22}	5×10^{17} Pa s for 2791–2891 km depth	$(dT/dz)_u$, $(dT/dz)_l = 0$
CON2c	10^{21}	5×10^{16} Pa s for 2791–2891 km depth	$(dT/dz)_u$, $(dT/dz)_l = 0$
CON2d	10^{21}	10^{17} Pa s for 2791–2891 km depth	$(dT/dz)_u$, $(dT/dz)_l = 0$

Fig. 9 shows the results for such models. The viscosity profiles for CON1a with $\eta_{CMB} = 10^{16}$ Pa s are shown in Fig. 9a and b shows the decay times for several such models. The predicted decay times for these models are shorter than 60 years as also predicted for the same sorts of TBL model. The η^*_{CMB}-values for models satisfying observationally inferred decay time are $\eta^*_{CMB} \geqslant 5 \times 10^{17}$ Pa s for CON1a and $\eta^*_{CMB} \geqslant 3 \times 10^{18}$ Pa s for CON1b ($\eta_{CMB} = 10^{17}$ *Pa s*). Among these permissible viscosity models, the model of CON1a with $\eta^*_{CMB} \sim 10^{18}$ Pa s can also explain geodetically inferred deformations for periods longer than ~0.1 year and produces the decay time ~40 years (Fig. 9c and d). We obtain a similar conclusion about the viscosity structure for viscosity models with $\eta_{top} = 10^{21}$ - Pa s. Such a conclusion has also been derived from TBL models of TBL1a and TBL2a (see Fig. 3). Consequently, these results for temperature-dependent viscosity models, for both TBL and CON models, indicate that the viscosity at the bottom of the D″ layer is ~10^{16} Pa s for $\eta_{top} = 10^{21}$ and 10^{22} Pa s.

Finally, we show the results for viscosity models with the lower layer of constant viscosity (η_{CMB}), in which the η_{CMB}-values for models with $\eta_{top} = 10^{22}$ Pa s are 5×10^{16}, 10^{17}, 2×10^{17} and 5×10^{17} Pa s for CON1c, CON1d, CON1e and CON1f models (Table 2), respectively. The decay times for CON1f are smaller than the observationally inferred values (Fig. 10b). The results shown in Fig. 10b–d indicate that the predictions for CON1d model with $2 \times 10^{17} < \eta^*_{CMB} \leqslant 10^{18}$ Pa s can explain both observationally inferred estimates, which is also true for CON1c model. In particular, the predicted decay times for CON1c model with η^*_{CMB} ~(5–10) $\times 10^{17}$ Pa s and for CON1d model with $\eta^*_{CMB} \sim 10^{18}$ Pa s are ~70 years for the optimum estimate by Wilson and Vicente (1990). These conclusions are also applicable to models with $\eta_{top} = 10^{21}$ Pa s.

We briefly state the results for the D″ layer model with 200 km thickness, in which the upper and lower layers have 50 km thickness and the interlayer has 100 km. In these models, the permissible viscosity ranges satisfying observationally inferred decay times and $k_r^{T,P}$ are $\eta^*_{CMB} > 5 \times 10^{17}$ Pa s and $\eta^*_{CMB} < 10^{17}$ Pa s, respectively. That is, we could not find permissible viscosity model satisfying both data sets even if we consider a 50 km constant low viscosity layer at the base of the D″ layer.

5. Implications for the D layer and core–mantle boundary region

We summarize the numerical results for TBL and CON models in Table 3. Viscosity models of the D″ layer satisfying observationally inferred decay times of the Chandler wobble and $k_r^{T,P}$ (amplitude response) for periods longer than ~0.1 year require either following condition: (i) temperature gradient is nearly constant for TBL model with the D″ layer of ~200 km thickness, (ii) temperature gradient of the lower part (~100 km thickness) is larger than that of the upper part for TBL model (D″ layer with 200 or 300 km thickness) and for CON model (D″ layer with 300 km thickness) and the CMB viscosity (η_{CMB}) is ~10^{16} Pa s for both models, and (iii) viscosity of the lower part (~100 km thickness) is constant and smaller than ~10^{17} Pa s for TBL model (D″ layer with 200 or 300 km thickness) and for

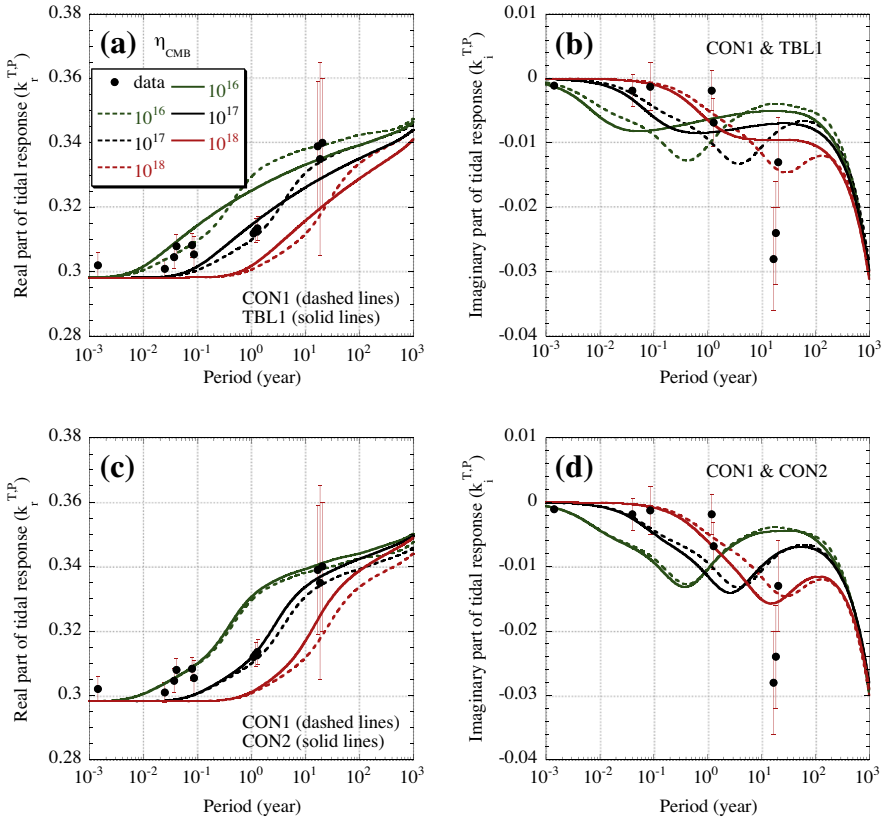

Fig. 8. Real (a, c) and imaginary (b, d) parts of tidal responses for CON1 and CON2 models as a function of period.

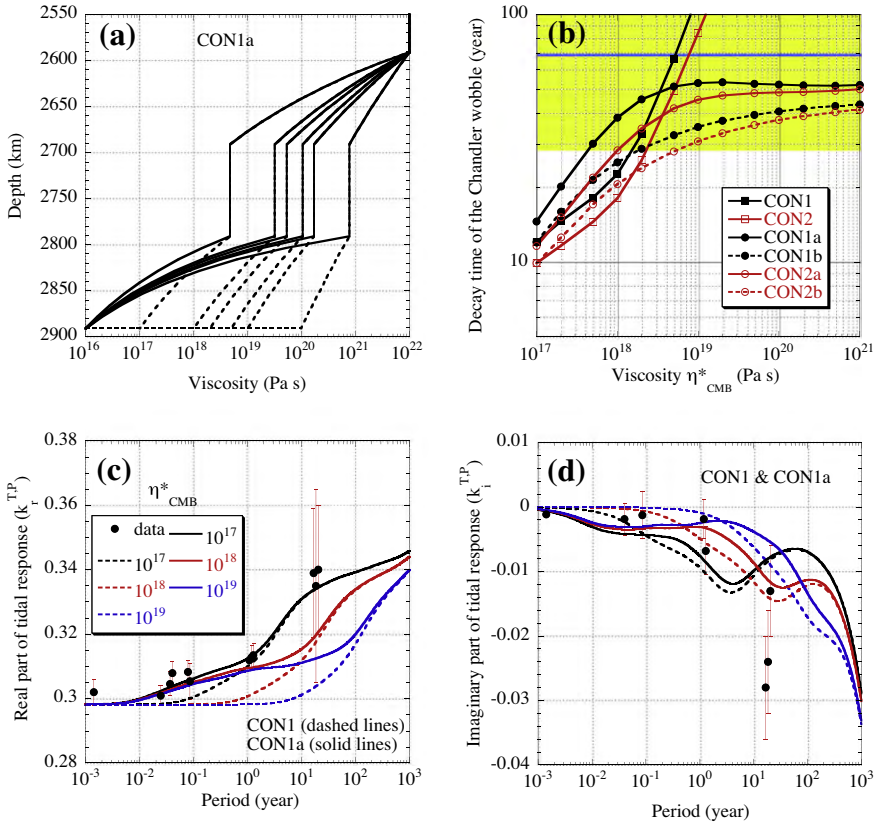

Fig. 9. Results of viscosity models for convecting D″ layer model. The thickness of the D″ layer is 300 km, and the thicknesses of upper thermal boundary layer, isothermal layer and bottom thermal boundary layer are 100 km. (a) Viscosity profiles for CON1a model, (b) decay times of the Chandler wobble as a function of η^*_{CMB} (see text), and real (c) and imaginary (d) parts of tidal responses as a function of period. The parameter values for each model are shown in Table 2.

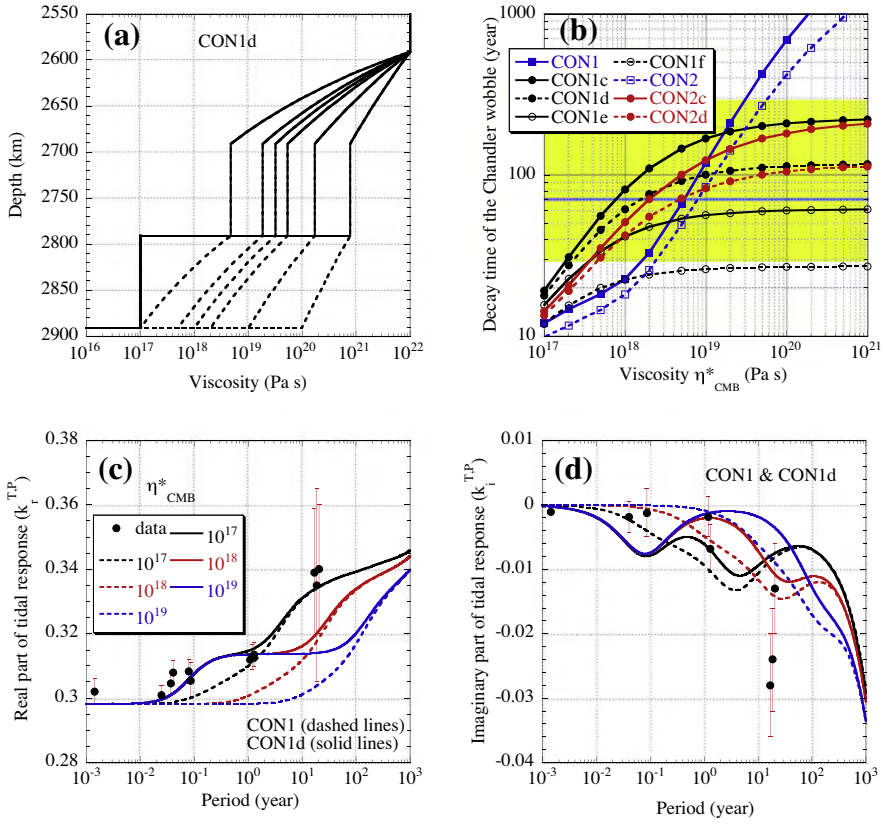

Fig. 10. Results for viscosity models with a constant low viscosity layer at the bottom of the D″ layer. The thicknesses of the D″ layer and the constant viscosity layer are 300 and 100 km, respectively, and those for upper thermal boundary layer and isothermal layer are 100 km. (a) Viscosity profiles for CON1d model, (b) decay times of the Chandler wobble as a function of η^*_{CMB} (see text), and real (c) and imaginary (d) parts of tidal responses as a function of period. The parameter values for each model are shown in Table 2.

CON model (D″ layer with 300 km thickness). Fig. 11 also shows the preferred viscosity structures of the D″ layer derived from our numerical experiments, in which the region with viscosity larger than $\sim 5 \times 10^{20}$ Pa s insignificantly affects the decay of the Chandler wobble (Nakada and Karato, 2012). The predicted $k_i^{T,P}$ for models satisfying the condition (ii) or (iii) also explains the observationally inferred value for 18.6 years tide, but TBL4 and TBL5 models with the D″ layer of 200 km thickness cannot explain the observationally inferred $k_i^{T,P}$ value for 18.6 years tide. However, if we consider that the phase response at 18.6 year tide may be explained by the electromagnetic coupling at the core–mantle boundary (Buffett et al., 2002) and is also highly sensitive to correction factors (Benjamin et al., 2006), then such models (TBL4 and TBL5) would be possible viscosity structures of the D″ layer.

We first discuss the temperature increase within the D″ layer (ΔT_{CMB}) for TBL4 and TBL5 models (see Fig. 11a) with the predicted decay times of ~30 years, which may correspond to the 'hot' mantle by Hernlund et al. (2005). These models require the CMB viscosity (η_{CMB}) of $\sim 10^{16}$ Pa s. The relationship between H^*/RT_{top} and $\Delta T_{CMB}/T_{top}$ using Eq. (6) is shown in Fig. 12 as a function of η_{CMB}. The permissible values of H^*/RT_{top} are 20–30 (Karato, 2008) and its values for H^* = 500 kJ mol^{-1} and T_{top} = 2600 K are 23.1. The estimates of ΔT_{CMB} derived from the relationship for $\eta_{CMB} = 10^{16}$ Pa s are as follows: (0.85–2.2) T_{top} for $\eta_{top} = 10^{22}$ Pa s and (0.6–1.3) T_{top} for $\eta_{top} = 10^{21}$ Pa s. If we assume T_{top} = 2600 K, then ΔT_{CMB} are larger than ~2200 K for $\eta_{top} = 10^{22}$ Pa s and larger than ~1500 K for $\eta_{top} = 10^{21}$ Pa s, in which the temperatures of 2200 K and 1500 K correspond to $H^*/RT_{top} \sim 30$. Recent estimates of the temperature at the top of the core (T_{CMB}), which are inferred from the iron melting temperature determinations for the inner-core boundary (Boehler, 2000; Alfè et al., 2002), are 3300–4300 K (see also Hernlund et al. (2005) and Lay et al. (2008)). Then, ΔT_{CMB} ~1500 K for $\eta_{top} = 10^{21}$ Pa s and T_{top} of 2700–2800 K may be a possible solution (TBL5 in Fig. 11a), which may correspond to the 'warm' mantle by Lay et al. (2008). If we also assume a commonly used estimate of thermal conductivity of 10 W m^{-1} K^{-1} (Stacey, 1992), then the average heat flow from the core to the mantle is estimated to be ~11 TW, 3–4 times larger than the estimate of ~3 TW by Stacey (1992). The temperature increase of ~1500 K is also obtained for models of TBL2a and CON2a for the D″ layer with 300 km thickness, which, however, correspond to the 'cold' mantle by Lay et al. (2008). The average heat flow for these models is 7–8 TW, 2–3 times larger than the estimate by Stacey (1992). That is, viscosity models with no constant low viscosity layer at the base of the D″ layer require high temperature increase of ~1500 K within the D″ layer and also suggest significantly high core heat flow larger than ~3 TW estimated by Stacey (1992).

We next discuss geophysical implications derived from the viscosity structures with a constant (channel-like) low viscosity layer at the base of the D″ layer such as TBL4c, TBL5c, TBL1d, TBL2d, CON1d and CON2d (see Fig. 11). These models with the D″ layer of 300 km thickness explain both data sets and also predict the decay time of the Chandler wobble similar to the optimum value by Wilson and Vicente (1990) (see Table 3). It is difficult to estimate the temperature increase within the D″ layer for these models. However, the minimum value may be inferred from the preferred extrapolated CMB viscosity, η^*_{CMB} (see, for example, Fig. 5a). The η^*_{CMB}-values for TBL4c and TBL5c are $\sim 10^{16}$ Pa s, and

Table 3
Summaries of the results based on TBL and CON models. The permissible viscosity ranges satisfying observationally inferred estimates are given by η_{CMB}-value for TBL1, TBL2, TBL4, TBL5, CON1 and CON2 models and η^*_{CMB}-value for other models.

Model name	Permissible viscosity range for τ_{CW} (Pa s)	Viscosity for optimum $\tau_{CW} \sim 70$ years (Pa s)	Permissible viscosity range for $k_r^{T,P}$ at periods longer than ~0.1 year (Pa s)	Permissible viscosity range satisfying τ_{CW} and $k_r^{T,P}$ for periods longer than ~0.1 year (Pa s), and optimum (or near optimum) τ_{CW} (year) and its viscosity (Pa s) (within the parenthesis)	Does the permissible viscosity range satisfying τ_{CW} and $k_r^{T,P}$ also satisfy $k_r^{T,P}$ for 18.6 years tide?
TBL1	2.5×10^{18}–4×10^{19}	$\sim 8 \times 10^{18}$	$\sim 10^{17}$	None	No
TBL2	3×10^{18}–7×10^{19}	$\sim 10^{19}$	$\sim 10^{17}$	None	No
TBL4	1.5×10^{18}–2.5×10^{19} 10^{16}~2×10^{16}	$\sim 5 \times 10^{18}$	10^{16}–10^{17}	$\sim 10^{16}$ (~30 yr for $\sim 10^{16}$ Pa s)	No
TBL5	2×10^{18}–4×10^{19} $\sim 10^{16}$	$\sim 6 \times 10^{18}$	10^{16}–10^{17}	$\sim 10^{16}$ (~30 yr for $\sim 10^{16}$ Pa s)	No
TBL1a	$\geqslant 7 \times 10^{17}$	None	10^{17}–10^{18}	$\sim 10^{18}$ (~30 yr for $\sim 10^{18}$ Pa s)	Yes
TBL1b	$\geqslant 6 \times 10^{18}$	None	10^{17}–10^{18}	None	No
TBL2a	$\geqslant 1.5 \times 10^{18}$	None	10^{17}–2×10^{18}	$\sim 2 \times 10^{18}$ (~30 yr for $\sim 2 \times 10^{18}$ Pa s)	Yes
TBL2b	$\geqslant 1.5 \times 10^{19}$	None	10^{17}–2×10^{18}	None	No
TBL1c	$\geqslant 2 \times 10^{17}$	$\sim 10^{18}$	10^{17}–10^{18}	2×10^{17}–10^{18} (~70 yr for $\sim 10^{18}$ Pa s)	Yes
TBL1d	$\geqslant 3 \times 10^{17}$	$\sim 2 \times 10^{18}$	10^{17}–2×10^{18}	3×10^{17}–2×10^{18} (~70 yr $\sim 2 \times 10^{18}$ Pa s)	Yes
TBL2c	$\geqslant 4 \times 10^{17}$	$\sim 2 \times 10^{18}$	2×10^{17}–2×10^{18}	3.5×10^{17}–2×10^{18} (~70 yr for $\sim 2 \times 10^{18}$ Pa s)	Yes
TBL2d	$\geqslant 5 \times 10^{17}$	$\sim 5 \times 10^{18}$	2×10^{17}–2×10^{18}	5×10^{17}–2×10^{18} (~55 yr for $\sim 2 \times 10^{18}$ Pa s)	Yes
TBL4c	$\geqslant 10^{16}$	$\sim 7 \times 10^{16}$	10^{16}~5×10^{16}	10^{16}–5×10^{16} (~60 yr for $\sim 5 \times 10^{16}$ Pa s)	No
TBL4d	$\geqslant 10^{16}$	$\sim 1.5 \times 10^{17}$	10^{16}–5×10^{16}	10^{16}~5×10^{16} (~50 yr for $\sim 5 \times 10^{16}$ Pa s)	No
TBL5c	$\geqslant 10^{16}$	$\sim 1.5 \times 10^{17}$	10^{16}–10^{17}	10^{16}–10^{17} (~60 yr for $\sim 10^{17}$ Pa s)	No
TBL5d	$>2 \times 10^{16}$	$\sim 4 \times 10^{17}$	2×10^{16}–10^{17}	2×10^{16}–10^{17} (~50 yr for 10^{17} Pa s)	No
CON1	1.5×10^{18}–3×10^{19}	$\sim 5 \times 10^{18}$	5×10^{17}–10^{18}	None	No
CON2	2.5×10^{18}–6×10^{19}	$\sim 8 \times 10^{18}$	5×10^{17}–2×10^{18}	None	No
CON1a	$\geqslant 5 \times 10^{17}$	None	10^{17}–10^{18}	5×10^{17}–10^{18} (~40 yr for $\sim 10^{18}$ Pa s)	Yes
CON1b	$\geqslant 2.5 \times 10^{18}$	None	10^{17}–10^{18}	None	No
CON2a	$>10^{18}$	None	10^{17}–2×10^{18}	10^{18}–2×10^{18} (~35 yr for $\sim 2 \times 10^{18}$ Pa s)	Yes
CON2b	$>8 \times 10^{18}$	None	10^{17}–2×10^{18}	None	No
CON1c	$\geqslant 2 \times 10^{17}$	$\sim 7 \times 10^{17}$	10^{17}–10^{18}	2×10^{17}–10^{18} (~70 yr for $\sim 7 \times 10^{17}$ Pa s)	Yes
CON1d	$>2 \times 10^{17}$	$\sim 1.5 \times 10^{18}$	10^{17}–10^{18}	2×10^{17}–10^{18} (~60 yr for $\sim 10^{18}$ Pa s)	Yes
CON2c	$\geqslant 4 \times 10^{17}$	$\sim 2 \times 10^{18}$	10^{17}–2×10^{18}	4×10^{17}–2×10^{18} (~70 yr for $\sim 2 \times 10^{18}$ Pa s)	Yes
CON2d	$\geqslant 5 \times 10^{17}$	$\sim 5 \times 10^{18}$	10^{17}–2×10^{18}	5×10^{17}–2×10^{18} (~55 yr for $\sim 2 \times 10^{18}$ Pa s)	Yes

the results are similar to those for TBL4 and TBL5. Those for models with 300 km thickness are $\eta^*_{CMB} \sim (1\text{–}2) \times 10^{18}$ Pa s for $\eta_{top} = 10^{22}$ and 10^{21} Pa s. Then, the estimates for ΔT_{CMB} (Fig. 12) are as follows: (0.4–0.8) T_{top} for $\eta_{top} = 10^{22}$ Pa s and (0.3–0.5) T_{top} for $\eta_{top} = 10^{21}$ Pa s. If we assume $T_{top} = 2600$ K, then ΔT_{CMB} are 1000–2100 K for $\eta_{top} = 10^{22}$ Pa s and 800–1300 K for $\eta_{top} = 10^{21}$ Pa s. For $H^* = 500$ kJ mol^{-1} ($H^*/RT_{top} = 23.1$), $\Delta T_{CMB} \sim 1600$ K and $T_{CMB} \sim 4200$ K for $\eta_{top} = 10^{22}$ Pa s and $\Delta T_{CMB} \sim 1000$ K and $T_{CMB} \sim 3700$ K for $\eta_{top} = 10^{21}$ Pa s, and the average heat flows are ~8 and ~5 TW, respectively, which are also larger than 3 TW.

These models have a constant (channel-like) low viscosity layer at the base of the D″ layer with ~100 km thickness and its viscosity smaller than $\sim 10^{17}$ Pa s. This layer may be related to the ultralow-velocity zone (ULVZ) detected just above the CMB in piles or layers a few tens of kilometers thick (Ganero et al., 1998). Hernlund and Jellinek (2010) argued that melt with a different density than the surrounding materials could be dynamically supported by flow (see also Lay et al., 2008). Such a mechanism is, however, highly sensitive to the viscosity, and therefore it would be necessary to examine the validity in the case of $\sim 10^{17}$ Pa s for the bottom part (~100 km thickness) viscosity of the D″ layer. Similarly, Kanda and Stevenson (2006) suggested that iron-rich melt may penetrate into the mantle by the pressure gradient caused by the dynamic topography. The depth of penetration of iron-rich melt is again controlled by the viscosity of the bottom of the D″ layer, and the penetration depth will be negligible (<1 m) if the viscosity there is less than 10^{18} Pa s as suggested by this study.

6. Conclusions

We have examined the decay time of the Chandler wobble and semi-diurnal to 18.6 years tidal deformations to estimate the temperature-dependent viscosity structure of the D″ layer. The temperature distribution depends on its dynamic state, and we therefore adopt two typical models, i.e., bottom thermal boundary layer of the mantle convection (TBL model) and vigorously small-scale convecting layer (CON model). In these models, we assume the viscosity at the top of the D″ layer η_{top} to be 10^{21} and 10^{22} Pa s. However, the choice of the viscosity at the top of the D″ layer does not affect the conclusion on the viscosity structure so much.

Three possible models are derived from the comparison between the numerical and observationally inferred decay times of Chandler wobble and tidal deformations. The first model corresponds to nearly constant temperature gradient within the D″ layer with its thickness (L) of 200 km in TBL model, and the viscosity at the CMB (η_{CMB}) is $\sim 10^{16}$ Pa s. The temperature increase within the D″ layer ΔT_{CMB} is larger than ~1500 K, and the temperature at the top of the core T_{CMB} corresponds to the recent estimate of 3300–4300 K. The second model requires that the temperature gradient of the lower part (~100 km thickness) is larger than that of the upper part and the $\eta_{CMB} \sim 10^{16}$ Pa s in TBL and CON models with $L = 300$ km. The temperature distribution causes a more distinct low viscosity zone at the base of the D″ layer, and ΔT_{CMB} is also larger than ~1500 K. The third model has a channel-like (constant)

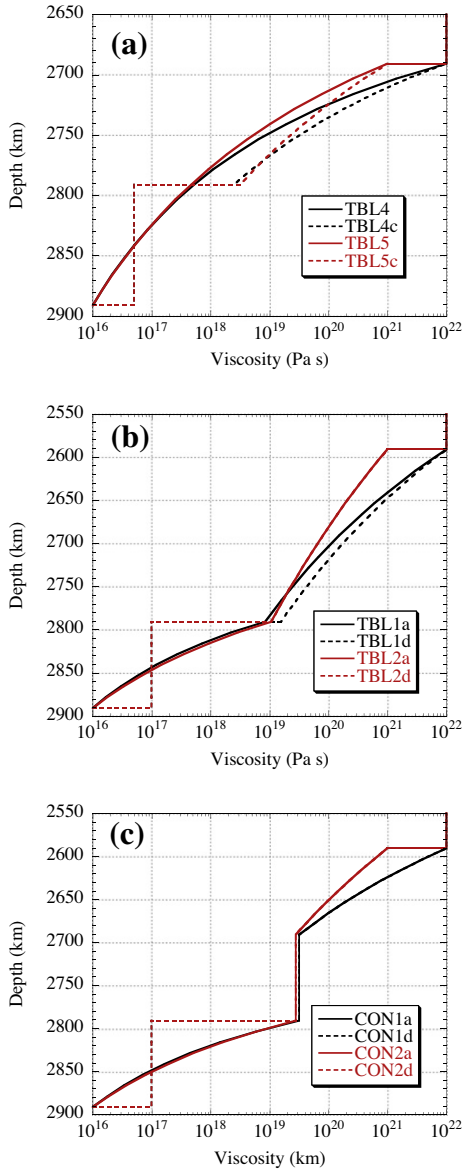

Fig. 11. Preferred viscosity structures of the D″ layer obtained in this study: (a) for TBL model with the thickness of 200 km, (b) for TBL model with 300 km thickness and (c) for CON model with 300 km thickness.

low viscosity layer (~100 km thickness) at the bottom of the D″ layer with its viscosity smaller than $\sim 10^{17}$ Pa s in TBL (L = 200 and 300 km) and CON (L = 300 km) models. The plausible estimates for the temperature increase are ~1600 K for $\eta_{top} = 10^{22}$ Pa s and ~1000 K for $\eta_{top} = 10^{21}$ Pa s. The heat flows from the core to the mantle for these three models appear to be significantly larger than ~3 TW estimated by Stacey (1992).

Among these three models, the predicted decay times for the first and second models are close to the minimum estimate (~30 years) by Wilson and Vicente (1990) and those for the third model are ~70 years corresponding to the optimum estimate. Also, the third model explains the geodetically inferred real (amplitude) and imaginary (phase lag) parts for the tidal deformations for periods longer than ~0.1 year. Consequently, the third model is a preferred model within the limited range of our numerical experiments. It would be important to examine the relationship between the channel-like low viscosity layer and the ultralow-velocity zone.

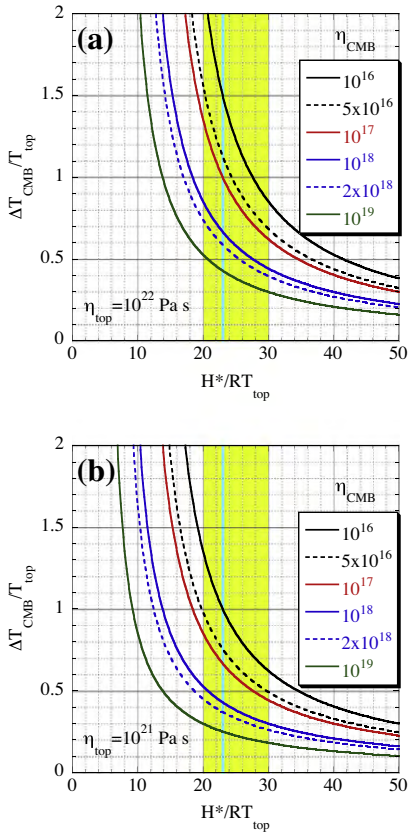

Fig. 12. The relationship between H^*/RT_{top} and $\Delta T_{CMB}/T_{top}$ using Eq. (6) as a function of η_{CMB}: (a) for $\eta_{top} = 10^{22}$ Pa s and (b) for $\eta_{top} = 10^{21}$ Pa s.

Acknowledgments

We thank H. Cizkova and an anonymous reviewer for their helpful comments. This work was partly supported by the Japanese Ministry of Education, Science and Culture (Grand-in-Aid for Scientific Research No. 22540440), and partly by the National Science Foundation of USA (to SK).

References

Alfè, D., Gillan, M.J., Price, G.D., 2002. Composition and temperature of the Earth's core constrained by combining ab initio calculations and seismic data. Earth Planet. Sci. Lett. 195, 91–98.
Benjamin, D., Wahr, J., Ray, R.D., Egbert, G.D., Sesai, S.D., 2006. Constraints on mantle anelasticity from geodetic observations, and implications for the J_2 anomaly. Geophys. J. Int. 165, 3–16.
Boehler, R., 2000. High-pressure experiments and the phase diagram of lower mantle and core constituents. Rev. Geophys. 38, 221–245.
Buffett, B.A., Mathews, P.M., Herring, T.A., 2002. Modeling of nutation and precession: effects of electromagnetic coupling. J. Geophys. Res. 107. http://dx.doi.org/10.1029/2000JB000056.
Dickman, S.R., Nam, Y.S., 1998. Constraints on Q at long periods from Earth's rotation. Geophys. Res. Lett. 25, 211–214.
Dziewonski, A.M., Anderson, D.L., 1981. Preliminary reference Earth model (PREM). Phys. Earth Planet. Inter. 25, 297–356.
Furuya, M., Chao, B.F., 1996. Estimation of period and Q of the Chandler wobble. Geophys. J. Int. 127, 693–702.
Garnero, E.J., Revenaugh, J., Williams, Q., Lay, T., 1998. Ultralow velocity zone at the core–mantle boundary. In: Gurnis, M., Wysession, M.E., Knittle, E., Buffett, B.A. (Eds.), The Core-Mantle Boundary Region, Geodynamics Series, vol. 28, American Geophysical Union, pp. 319–334.
Gross, R.S., 2007. Earth rotation variations – long periods. In: Herring, T. (Ed.), Treatise on Geophysics, vol. 3. Geodesy, Elsevier, pp. 239–294.
Hager, B.H., 1984. Subducted slabs and the geoid: constraints on mantle rheology and flow. J. Geophys. Res. 89, 6003–6015.
Hager, B.H., Clayton, R.W., Richards, M.A., Comer, R.P., Dziewonski, A.M., 1985. Lower mantle heterogeneity, dynamic topography and the geoid. Nature 313, 541–545.

Hernlund, J.W., Thomas, C., Tackley, P.J., 2005. A dounbling of the post-perovskite phase boundary and structure of the Earth's lowermost mantle. Nature 434, 882–886.
Hernlund, J.W., Jellinek, A.M., 2010. Dynamics and structure of a stirred partially molten ultralow-velocity zone. Earth Planet. Sci. Lett. 296, 1–8.
Kanda, R.V.S., Stevenson, D.J., 2006. Suction mechanism for iron entrainment into the lower mantle. Geophys. Res. Lett. 33. http://dx.doi.org/10.1029/2005GL025009.
Karato, S., 2008. Deformation of Earth Materials: An Introduction to the Rheology of Solid Earth. Cambridge University Press, Cambridge.
Karato, S., Karki, B.B., 2001. Origin of lateral heterogeneity of seismic wave velocities and density in Earth's deep mantle. J. Geophys. Res. 106, 21771–21783.
Lambeck, K., Nakiboglu, S.M., 1983. Long-period Love numbers and their frequency dependence due to dispersion effects. Geophys. Res. Lett. 10, 857–860.
Lay, T., Hernlund, J., Buffett, B., 2008. Core–mantle boundary heat flow. Nature Geosci. 1, 25–32.
Mitrovica, J.X., Peltier, W.R., 1991. Radial resolution in the inference of mantle viscosity from observations of glacial isostatic adjustment. In: Sabadini, R., Lambeck, K., Boschi, E. (Eds.), Glacial Isostasy, Sea-Level and Mantle Rheology. Kluwer Academic Publisher, Dortrecht, pp. 63–78.
Mitrovica, J.X., Forte, A.M., 2004. A new inference of mantle viscosity based upon joint inversion of convection and glacial isostatic adjustment data. Earth Planet. Sci. Lett. 225, 177–189.
Munk, W.H., MacDonald, G.J.F., 1960. The Rotation of the Earth: a Geophysical Discussion. Cambridge University Press, Cambridge.
Nakada, M., 2009. Polar wander of the Earth associated with the Quaternary glacial cycle on a convecting mantle. Geophys. J. Int. 179, 569–578.
Nakada, M., Lambeck, K., 1989. Late Pleistocene and Holocene sea-level change in the Australian region and mantle rheology. Geophys. J. 96, 497–517.
Nakada, M., Karato, S., 2012. Low viscosity of the bottom of the Earth's mantle inferred from the analysis of Chandler wobble and tidal deformation. Phys. Earth Planet. Inter. 192–193, 68–80.
Peltier, W.R., 1974. The impulse response of a Maxwell Earth. Rev. Geophys. Space Phys. 12, 649–669.
Peltier, W.R., Andrews, J.T., 1976. Glacial-isostatic adjustment: I. The forward problem. Geophys. J. R. Astr. Soc. 46, 605–646.
Ray, R.D., Eanes, R.J., Lemoine, F.G., 2001. Constraints on energy dissipation in the Earth's body tide from satellite tracking and altimetry. Geophys. J. Int. 144, 471–480.
Sabadini, R., Peltier, W.R., 1981. Pleistocene deglaciation and the Earth's rotation: implications for mantle viscosity. Geophys. J. R. Astr. Soc. 66, 553–578.
Sabadini, R., Yuen, D.A., Widmer, R., 1985. Constraints on short-term mantle rheology from the $\dot{J}_2$ observation and dispersion of the 18.6 y tidal Love number. Phys. Earth Planet. Inter. 38, 235–249.
Smith, M.L., Dahlen, F.A., 1981. The period and Q of the Chandler wobble. Geophys. J. R. Astr. Soc. 64, 223–281.
Solomatov, V.S., Moresi, L.N., 2002. Small-scale convection in the D″ layer. J. Geophys. Res. 107. http://dx.doi.org/10.1029/2000JB000063.
Stacey, F.D., 1992. Physics of the Earth. Brookfield Press, Brisbane.
Turcotte, D.L., Schubert, G., 1982. Geodynamics. John Wiley & Sons, New York.
Vicente, R.O., Wilson, C.R., 1997. On the variability of the Chandler frequency. J. Geophys. Res. 102, 20439–20445.
Wilson, C.R., Vicente, R.O., 1990. Maximum likelihood estimates of polar motion parameters. In: McCarthy, D.D., Carter, W.E. (Eds.), Variations in Earth Rotation, AGU Geophys. Monogr. 59, American Geophysical Union, pp. 151–155.
Wu, P., Peltier, W.R., 1984. Pleistocene deglaciation and the Earth's rotation: a new analysis. Geophys. J. R. Astr. Soc. 76, 753–791.
Yamazaki, D., Karato, S., 2001. Some mineral physics constraints on the rheology and geothermal structure of Earth's lower mantle. Am. Mineral. 86, 385–391.